ARTICLE IN PRESS

Deep-Sea Research II ∎ (∎∎∎∎) ∎∎∎–∎∎∎

Contents lists available at ScienceDirect

Deep-Sea Research II

journal homepage: www.elsevier.com/locate/dsr2

The potential role of sea ice melt in the distribution of chromophoric dissolved organic matter in the Chukchi and Beaufort Seas

Christie L. Logvinova [a], Karen E. Frey [a,*], Lee W. Cooper [b]

[a] Graduate School of Geography, Clark University, Worcester, MA, USA
[b] University of Maryland Center for Environmental Science, Solomons, MD, USA

ARTICLE INFO

Keywords:
Chromophoric dissolved organic matter (CDOM)
Dissolved organic matter (DOM)
Sea ice
Arctic
Biogeochemistry

ABSTRACT

We investigated chromophoric dissolved organic matter (CDOM) in sea ice and the underlying water column in the Chukchi and Beaufort seas of the Pacific Arctic region and its relationship with both physical and biogeochemical parameters. Sea ice, water and melt pond samples were collected as sea ice melted in June–July 2010 and 2011. CDOM absorption was found to be significantly lower in sea ice compared to under-ice waters. In particular, the average CDOM absorption coefficient at 254 nm was approximately four times greater in the underlying water column than in the overlying ice. This indicates that melting sea ice did not contribute to net CDOM at this point in the melt season, but rather diluted CDOM in the under-ice water column. In the 2011 under-ice water column samples, the average CDOM absorption coefficients at 440 nm were twice as high along a transect associated with high phytoplankton biomass, which may have been contributed through subsequent microbial generation of CDOM. Less extensive sea ice cover with melt ponds may also have increased the presence of CDOM owing to increases in light transmission, leading to under-ice phytoplankton blooms and associated microbial production. However, oxygen isotope analysis of these waters with high under-ice phytoplankton biomass also indicates the presence of prior sea ice melt, including potentially sea ice algae and microbes, which could have also contributed to this anomalously high CDOM. These observations suggest that while melting sea ice may not necessarily contribute to increased CDOM concentrations, there are circumstances where CDOM in underlying waters may be higher than expected, either due to enhanced light transmission and higher under-ice production, and/or prior ice melt that provided significant contributions to under-ice CDOM.

1. Introduction

Arctic seasonal sea ice extent has significantly decreased in recent years (Serreze et al., 2007; Stroeve et al., 2007; Comiso et al., 2008; Perovich et al., 2012). This has been accompanied by an increase in the length of the summer melt season (Markus et al., 2009) and an overall thinning of the ice pack (Maslanik et al., 2007, Kwok and Rothrock, 2009; Maslanik et al., 2011; Comiso, 2012). Arctic sea ice is expected to continue thinning and decreasing in areal extent, but there are large uncertainties as to how this will impact biological and biogeochemical processes in the Arctic Ocean. One uncertainty with this sea ice decline is how and to what extent chromophoric dissolved organic matter (CDOM) in underlying ocean waters will be impacted. CDOM plays an important role in the marine ecosystem by inhibiting light transmittance through the water column and providing a food source for aquatic bacteria (Moran and Zepp, 1997; Blough and Del Vecchio, 2002; Nelson and Siegel, 2002). Although CDOM has been observed in Arctic sea ice (Belzile et al., 2000; Scully and Miller, 2000; Stedmon et al., 2007a), its distribution is not well known, making it difficult to predict the impact of sea ice decline on biological and biogeochemical processes in the Arctic Ocean.

Sources of CDOM in the ocean include two primary categories: (a) *in situ* (autochthonous) biological production (*e.g.*, Carlson et al., 2002); and (b) inputs of terrestrially-derived (allochthonous) organic matter transported to the ocean by terrestrial runoff. CDOM is defined as the optically active fraction of dissolved organic material (DOM), absorbing ultraviolet (UV) and visible light, and acting as one of the primary regulators of light penetration in the oceanic euphotic zone (Blough and Del Vecchio, 2002; Nelson and Siegel, 2002). In particular, CDOM limits the amount of photosynthetically active radiation (PAR) in the water column, thereby potentially reducing rates of primary production

* Corresponding author.

http://dx.doi.org/10.1016/j.dsr2.2016.04.017
0967-0645/© 2016 Published by Elsevier Ltd.

(Retamal et al., 2008) but also blocking harmful UV radiation (Williamson et al., 2001). CDOM can also contribute to the heating of surface waters and subsequent melting of sea ice by absorbing shortwave visible radiation (380–760 nm; Kirk, 1988, 1994; Pegau, 2002; Granskog et al., 2007; Hill, 2008). In addition, absorption of light by CDOM can lead to photodegradation of DOM, potentially resulting in a decrease in CDOM absorption of light (i.e., photobleaching). Through these photodegradation processes, a pool of DOM can be directly photomineralized to dissolved inorganic carbon, with subsequent outgassing of CO_2 to the atmosphere (Xie and Gosselin, 2005; Belanger et al., 2006; Stubbins et al., 2008; Osburn et al., 2009). In addition, less bio-reactive (refractory) DOM may be broken down into more biologically labile material, allowing it to be more readily respired by bacterioplankton (Moran and Zepp, 1997).

In the polar regions, sea ice can be considered a potential source of CDOM to underlying ocean waters. During ice formation most of the CDOM from the underlying water column is removed from the ice during brine rejection, however, a small fraction of CDOM can be incorporated into the ice and later redistributed to the water column upon sea ice melt (Belzile et al., 2000, 2002; Amon et al., 2004; Dittmar, 2004; Matsuoka et al., 2012). Additionally, CDOM can be produced *in situ* within the ice by sea ice algae (Belzile et al. 2000; Scully and Miller, 2000).

Previous studies of the optical characteristics of CDOM in sea ice include work in the Baltic Sea (Ehn et al., 2004; Granskog et al., 2005; Stedmon et al., 2007a; Uusikivi et al., 2010), the Canadian Arctic (Belzile et al., 2000, Scully and Miller, 2000), and Antarctica (Norman et al., 2011). The magnitude of CDOM absorption in sea ice can be up to two orders of magnitude greater than that found in the adjacent water column in Baffin Bay (Scully and Miller, 2000) and up to four times greater than that found within sea ice brines in Antarctica (Norman et al., 2011). Scully and Miller (2000) concluded that sea ice is a significant source of CDOM during sea ice melt in Baffin Bay and Antarctic sea ice has also been implicated as a potential source of CDOM to ocean waters (Ortega-Retuerta et al., 2010, Norman et al., 2011).

In this study, we investigated CDOM properties of sea ice and the under-ice water column in the Chukchi and Beaufort Seas during sea ice melt in June–July 2010 and 2011. Specifically, we examined: (1) the optical properties of CDOM in the sea ice; (2) how this compares to CDOM in the under-ice water column; and (3) how sea ice melt could affect the distribution of CDOM in the underlying water. In addition to CDOM absorbance, spectral slope parameters were calculated to provide insight on DOM quality including molecular weight (Blough and Del Vecchio, 2002; Helms et al., 2008). Sea ice melt impacts on CDOM were investigated using oxygen isotope analyzes. While sea ice and meteoric water have similar salinities as a result of brine rejection during sea ice formation, fresh water from sea ice melt can be distinguished from meteoric waters because the latter is depleted in the heavier isotopes of oxygen (Dansgaard, 1964). We used the ratios of the oxygen isotopes, ^{18}O and ^{16}O, to assess the relative fractions of sea ice melt and meteoric water in under-ice waters, an approach that has been widely used in the Arctic (*e.g.* Ekwurzel et al., 2001; Cooper et al., 2005). A combination of fluorescence Excitation Emission Matrix (EEM) spectroscopy and Parallel Factor (PARAFAC) analyzes was used to provide additional information about the composition and potential sources of CDOM (Coble 1996; 2007; Stedmon and Bro, 2008). In addition, salinity, chlorophyll-*a* (Chl*a*) and the fluorescent portion of CDOM (FDOM) were used to investigate potential sources of CDOM in the underlying water column.

2. Study sites and methods

2.1. Study area

Ocean water and sea ice samples were collected as part of NASA's ICESCAPE (Impacts of Climate change on the Eco-Systems and Chemistry of the Arctic Pacific Environment) program in the Chukchi and Beaufort Seas during the summer melt season in June and July of 2010 and 2011 (Cruises HLY1001 and HLY1101 on the US Coast Guard Cutter (USCGC) *Healy*; Fig. 1). The overarching goal of this program was to better understand the impacts of climate change on the ecology and biogeochemistry of this biologically productive region through multidisciplinary observations of the biological, chemical, physical and optical properties of both the sea ice and the upper ocean during the summer melt season.

Sea ice and water samples were collected June 25–July 11, 2010 at 10 ice stations clustered north of Barrow, Alaska (Fig. 1). Samples were additionally collected at 9 ice stations distributed along three north-south ship transects between July 4–19, 2011 (Fig. 1). The westernmost transect (Transect 1) was located on the continental shelf of the Chukchi Sea in an area of high under-ice primary productivity (Arrigo et al., 2012, 2014), the central transect (Transect 2) crossed the shelf-basin interface in the Chukchi Sea, and the easternmost transect (Transect 3) extended into the Canada Basin of the Arctic Ocean from the shelf in a region impacted by river runoff, primarily from the Colville River.

2.2. Sampling

At each station, under-ice ocean water samples were collected by hand deploying a 2 L Kemmerer water sampler through holes drilled in the sea ice. Samples were collected at six depths below the ice: 0 m (ice–water interface), 1 m, 5 m, 10 m, 20 m, and 30 m. Additional water was also collected from a representative melt pond (from the sea ice surface) at each station. Two ice cores were taken at every site: one from bare ice and the second from below a melt pond. All ice cores were sub-sectioned into 10 cm increments and melted shipboard for subsequent analysis. Both water and melted sea ice samples were analyzed for salinity, CDOM, and $\delta^{18}O$ values. Additionally, under-ice waters from 2011 were analyzed for FDOM and Chl*a*. Salinity measurements were made shipboard using a Guildline Autosal salinometer, while Chl*a* measurements were made shipboard using a Turner Designs 10 AU field fluorometer. Samples for $\delta^{18}O$ were taken directly from the water sampler and melted ice. Samples for CDOM and FDOM (the fluorescent portion of CDOM) were filtered using pre-rinsed 0.2 μm Whatman Nuclepore polycarbonate track-etched membranes immediately after sampling. CDOM was determined shipboard, while samples for $\delta^{18}O$ (left unfrozen) were later analyzed at the University of Maryland Center for Environmental Science. FDOM was frozen and later analyzed on a spectrofluorometer. We note that ideally FDOM would have been measured shipboard within 24 h of sampling (Mitchell et al., 2003), however this was not practical due to the ship's ice breaking activities and resulting interference with the long integration time necessary to measure low FDOM intensity. For these reasons, samples were frozen and measured ashore.

2.3. Analyses

2.3.1. CDOM

After filtering, CDOM samples were stored in the dark at 4 °C in acid washed (10% HCl) pre-combusted (450 °C for 6 h) foil-covered Qorpak clear glass bottles (Bridgeville, Pensylvania, USA) and analyzed within 24 h. CDOM absorbance was measured using a Shimadzu UV-1800 UV–visible spectrophotometer at 1 nm

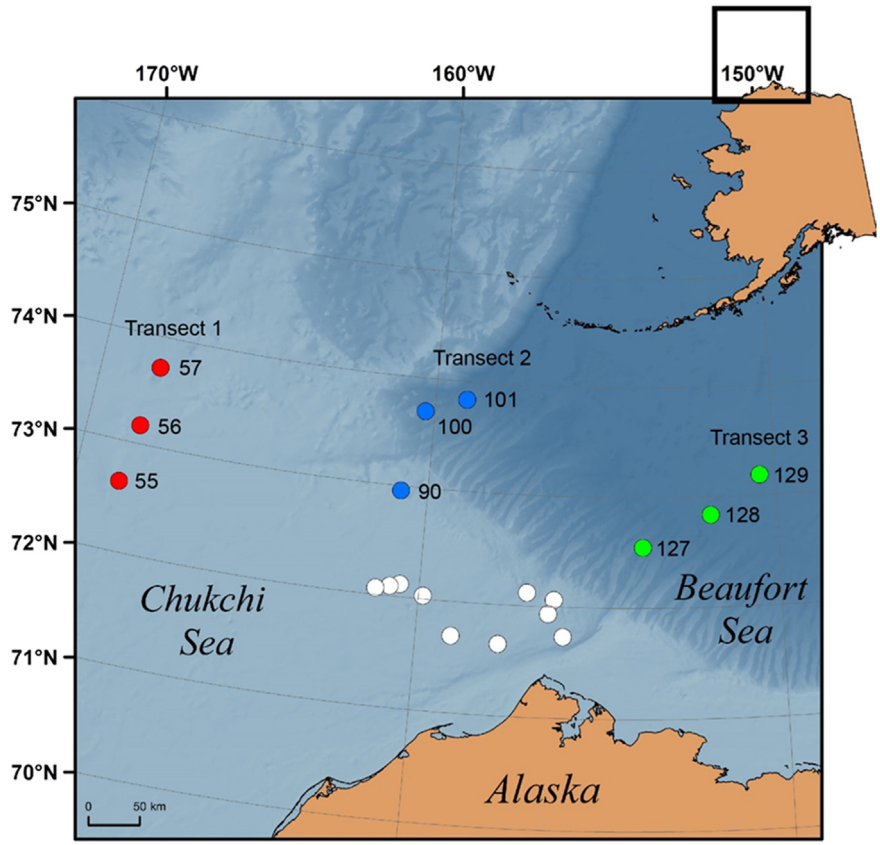

Fig. 1. Map of ice stations from 2010 and 2011 ICESCAPE cruises. Stations from 2010 are shown in white. Stations from 2011 are separated into three transects: Transect 1 (red), Transect 2 (blue), and Transect 3 (green). Background colors reflect bathymetry, with darker blue representing deeper waters (> 3000 m) in the Canada Basin. Lighter colors are shelf stations. (For interpretation of the references to color in this figure legend, the reader is referred to the web version of this article.)

intervals between 200 and 800 nm using a 10 cm quartz cuvette. All sample spectra were blank corrected and referenced against Milli-Q water (18 Ω). Measurements were made after samples had equilibrated to laboratory temperature in order to minimize temperature effects. CDOM absorbance was treated as zero above 750 nm, and the average absorbance between 750 nm and 800 nm was subtracted from the spectrum to correct for offsets owing to instrument baseline drift, temperature, scattering and refractive effects (Green and Blough, 1994; Helms et al., 2008). CDOM absorption coefficients were calculated from:

$$a(\lambda) = 2.303A(\lambda)/l \quad (1)$$

where a is the Naperian absorption coefficient (m^{-1}) at a specific wavelength (λ, in nanometers), A is the absorbance at the wavelength, and l is the cell path length in meters (Green and Blough, 1994). The detection limit is approximately $\pm 0.05\ m^{-1}$, based upon instrument specifications and characteristics.

The spectral slope (S, nm^{-1}) of each CDOM absorbance spectrum was calculated using a nonlinear fit of an exponential function,

$$a(\lambda) = a(\lambda_0)e^{-S(\lambda-\lambda_0)} \quad (2)$$

where $a(\lambda)$ is the absorption coefficient of CDOM (m^{-1}) at wavelength λ, and λ_0 the reference wavelength (in this case 250 nm). Slopes were calculated across the wavelength ranges of 275–295 nm and 350–400 nm. The spectral slope parameter provides insights on DOM molecular weight (Blough and Del Vecchio, 2002; Helms et al., 2008) and is largely independent of CDOM concentration (Brown, 1977). The 275–295 nm and 350–400 nm slope ranges were chosen because they have shown the greatest variation in a wide range of samples, including DOM-rich terrestrial, estuarine, coastal and highly photo-bleached waters (Helms et al., 2008). All slopes are reported here as positive numbers such that higher (i.e., steeper) slopes indicate a greater decrease in absorption with increasing wavelength.

2.3.2. FDOM

After slowly thawing and reaching room temperature, the fluorescent portion of CDOM (FDOM) for the 2011 under-ice water samples was measured using fluorescence Excitation Emission Matrix (EEM) spectroscopy on a Horiba Jobin-Yvon FluoroMax 4 spectrofluorometer, which creates three-dimensional structures composed of multiple emission spectra at a range of excitations and provides additional information about the chemical composition and sources of CDOM (Coble, 1996, 2007; Stedmon et al., 2003). EEMs were obtained by recording sample emission across 320–500 nm (with 2 nm increments) after excitation from 250 to 450 nm wavelengths (with 5 nm increments). Owing to low fluorescence intensities, samples were run using long integration periods (0.5 s) to minimize measurement noise. All EEMs were blank corrected and Raman calibrated (Lawaetz and Stedmon, 2009) using Milli-Q water spectra run on the same day. Finally, to eliminate Rayleigh scatter effects, zeros were inserted in the region where emission wavelengths are less than or equal to the excitation wavelength (+30 nm). The absorption coefficients of all samples were $< 10\ m^{-1}$, eliminating the need for inner filter corrections (Stedmon and Bro, 2008). It should be noted that the freezing process can cause flocculation that results in slightly higher CDOM absorbance values (Griffin et al., 2012). However, highly colored allochthonous-dominated DOM samples generally experience much greater effects of freeze/thaw than optically clearer autochthonous marine waters, and a number of studies

focused on marine DOM have shown minimal effects of freeze/thaw (outside of analytical error) on DOM optical properties (Spencer and Coble, 2014).

Many fluorescent components have overlapping peaks, making it difficult to identify individual components within an EEM. To identify independently varying FDOM components within our dataset, and to assess marine- vs. terrestrially-derived material, we conducted Parallel Factor (PARAFAC) analyses in MATLAB using the DOMFluor Toolbox following Stedmon and Bro (2008). In total, we included 54 EEMs: 6 samples for each of the 9 stations in 2011. To simplify the modeling process, we included only emission wavelengths from 320 to 476 nm in the EEMs. During the initial analyses, no EEMs were identified as outliers. A series of PARAFAC models (utilizing between 2 and 7 components) were applied and initial model fitting assessed using the steps as outlined in Stedmon and Bro (2008). Final model validation was conducted using random split half analysis and random initialization. Split half validation involves splitting the sample data into two halves and comparing model fits after running models on the two halves independently. Random initialization was then used to ensure that the models were in fact the least squares result and represented local minima.

2.3.3. Oxygen isotopes

Samples for $\delta^{18}O$ were stored 5 °C in small 20 mL borosilicate glass scintillation vials, with Polyseal® caps and wrapped in parafilm to limit evaporation and returned to the Chesapeake Biological Laboratory for analysis. Water samples were analyzed by equilibration with carbon dioxide using a Thermo Fisher Gas Bench peripheral linked to a Delta Plus stable isotope mass spectrometer run in continuous flow mode. Analysis of in-house water standards during sample analysis and calibration to international water isotope standards (V-SMOW, V-SLAP, GISP) indicated that analytical precision was better than ±0.1‰. Data corrections were made based upon analysis of the in-house standards relative to international standards, which were normalized per recommendations of Paul et al. (2007).

2.3.4. Chlorophyll-a (Chla)

Chl*a* was measured by filtering 250 ml water samples through 25 mm GF/F filters. The filters were initially frozen to fracture cell walls, and then stored in 10 ml of 90% acetone at 4 °C for 24 h in the dark. Extracted Chl*a* was measured using the Welschmeyer (1994) method with a Turner Designs 10 AU field fluorometer. The fluorometer was calibrated with a chlorophyll standard (Turner Designs Part No. 10-850) before and after all sampling, with use of a secondary solid standard (Part No.10-AU-904) during sampling to identify any possible instrument drift.

3. Results

3.1. CDOM optical properties

For most samples, the absorption spectra of CDOM followed the expected exponential decline with increasing wavelength (*e.g.*, Bricaud et al., 1981, Fig. 2). However, a small portion of samples had absorption spectra that differed from this typical exponential decay and instead exhibited distinct shoulders and peaks between 260 and 400 nm (Fig. 2). In 2010 the shoulders and peaks occurred in the sea ice cores and also in the under-ice water samples at 0 m (at the ice–water interface) and 1 m below the ice. In 2011 these anomalous patterns only occurred in the sea ice samples. In these samples, the degree of light absorption between 260 and 400 nm was substantially increased compared to the typical exponential decline observed in most CDOM samples (Fig. 2). We used the

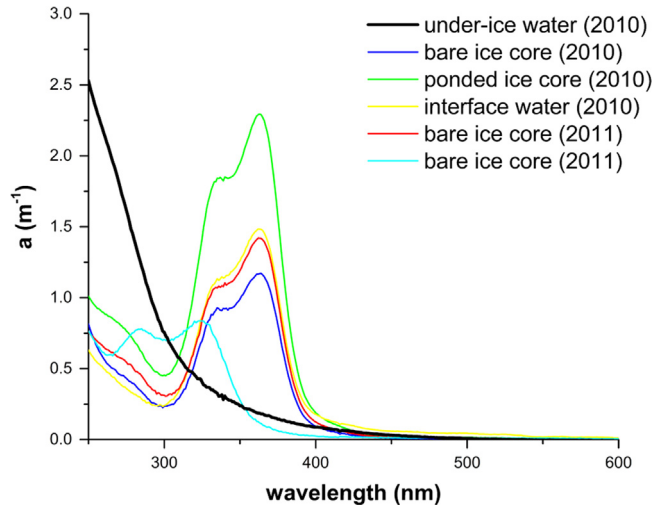

Fig. 2. Examples of CDOM absorption spectra exhibiting distinct shoulders and peaks between 260 and 400 nm compared to the typical exponential decline (black).

absorption coefficients at 254 nm (a_{254}) and 440 nm (a_{440}) to represent the background CDOM to avoid overestimating the relative CDOM concentrations in these samples due to the shoulders and peaks present between 260 and 400 nm.

Sea ice samples from ice cores below melt ponds and bare ice cores in both years had similar absorption coefficients and spectral slopes (Table 1 and Fig. 3). Absorption at 254 nm and 440 nm was similar in both years with an average absorption at 254 nm of 0.66 m^{-1} in 2010 and 0.57 m^{-1} in 2011 and an average absorption at 440 nm of 0.02 m^{-1} in 2010 and 0.01 m^{-1} in 2011. Spectral slopes were also similar between years. The average for $S_{275-295}$ was 0.029 in 2010 and 0.028 in 2011 and the average for $S_{350-400}$ was 0.026 in both years. In addition, optical properties were vertically consistent within each ice core (Fig. 3). Most of the outliers were in the 2010 bare ice cores where we sometimes observed higher a_{254}, a_{440}, and $S_{275-295,}$ but lower $S_{350-400}$ than average. In the 2011 cores, a few samples exhibited lower $S_{275-295}$ and higher $S_{350-400}$ than average.

Most DOM optical properties of the under-ice water samples were significantly different from those of the ice samples. Within each year, all optical properties were statistically different ($p < 0.05$) between ice core and under-ice water samples; however, when all ice samples were compared to all under-ice water samples from both years, $S_{275-295}$ was not statistically different ($p > 0.05$) between sample types. Overall, a_{254} and a_{440} were both higher ($p < 0.05$) in the under-ice water samples compared to the ice core samples, whereas $S_{350-400}$ was lower ($p < 0.05$) in the under-ice waters and $S_{275-295}$ was similar ($p > 0.05$) across all samples (Table 1). In particular, the average a_{254} value was approximately four times greater in the underlying water column than in the overlying ice.

DOM optical properties of the under-ice water samples showed some variation between years and in 2011 all DOM optical properties in Transect 1 were statistically different ($p < 0.05$) from the other two transects (Table 1, Fig. 4). a_{254} and $S_{350-400}$ in the under-ice water samples were similar ($p > 0.05$) between years. In contrast, a_{440} was higher ($p < 0.05$) and $S_{275-295}$ was lower ($p < 0.05$) in 2010 than in 2011. For both years, optical properties were relatively constant throughout much of the water column sampled (0–30 m) (Fig. 4), with variations typically occurring at the interface between the ocean water and the overlying sea ice (at our designated 0 m depth). Most of the DOM optical properties from the under-ice water column samples collected in 2011 from

Table 1
Physical and biogeochemical measurements of water and ice samples from 2010 and 2011, including both the mean (±1 SD) and total range of the measurements.

	2010 Water samples	2011 Water samples				2010 Ice samples			2011 Ice samples		
	All ($n=56$)	Transect 1 ($n=18$)	Transect 2 ($n=18$)	Transect 3 ($n=18$)	All ($n=54$)	Bare ice ($n=113$)	Melt pond ice ($n=54$)	All ($n=167$)	Bare ice ($n=93$)	Melt pond ice ($n=61$)	All ($n=154$)
a_{254} (m^{-1})	2.44 ± 0.63 (0.47–3.63)	2.29 ± 0.30 (1.72–2.69)	2.41 ± 0.18 (2.08–2.84)	2.37 ± 0.12 (2.13–2.61)	2.36 ± 0.22 (1.72–2.84)	0.68 ± 0.40 (0.10–2.49)	0.63 ± 0.33 (0.23–1.67)	0.66 ± 0.38 (0.10–2.49)	0.56 ± 0.13 (0.39–1.10)	0.57 ± 0.18 (0.32–1.20)	0.57 ± 0.15 (0.32–1.20)
a_{440} (m^{-1})	0.06 ± 0.03 (0.02–0.17)	0.07 ± 0.02 (0.05–0.10)	0.04 ± 0.02 (0.02–0.13)	0.03 ± 0.01 (0.02–0.04)	0.05 ± 0.02 (0.02–0.13)	0.02 ± 0.02 (0.00–0.11)	0.02 ± 0.01 (0.00–0.04)	0.02 ± 0.02 (0.00–0.11)	0.01 ± 0.01 (0.00–0.04)	0.01 ± 0.01 (0.00–0.05)	0.01 ± 0.01 (0.00–0.05)
$S_{(275-295)}$	0.028 ± 0.002 (0.022–0.037)	0.027 ± 0.002 (0.024–0.029)	0.032 ± 0.002 (0.026–0.034)	0.033 ± 0.001 (0.030–0.035)	0.031 ± 0.003 (0.024–0.035)	0.029 ± 0.006 (0.018–0.054)	0.029 ± 0.004 (0.023–0.038)	0.029 ± 0.005 (0.018–0.054)	0.028 ± 0.005 (0.000–0.034)	0.027 ± 0.005 (0.005–0.032)	0.028 ± 0.005 (0.000–0.034)
$S_{(350-400)}$	0.019 ± 0.003 (0.014–0.029)	0.017 ± 0.002 (0.014–0.019)	0.021 ± 0.002 (0.013–0.024)	0.021 ± 0.001 (0.019–0.023)	0.020 ± 0.003 (0.013–0.024)	0.025 ± 0.005 (0.003–0.036)	0.027 ± 0.005 (0.014–0.038)	0.026 ± 0.005 (0.003–0.038)	0.027 ± 0.007 (0.015–0.057)	0.025 ± 0.006 (0.014–0.056)	0.026 ± 0.006 (0.014–0.057)
Salinity	27.1 ± 7.8 (1.1 – 32.8)	30.6 ± 3.5 (17.4–32.9)	26.9 ± 2.1 (22.4–30.0)	25.8 ± 1.7 (20.8–28.0)	27.8 ± 3.3 (17.4–32.9)	1.6 ± 1 (0.0–3.4)	0.9 ± 0.6 (0.2–2.9)	1.4 ± 0.9 (0.0–3.4)	2.4 ± 0.9 (0.4–4.2)	2.0 ± 0.8 (0.7–3.6)	2.3 ± 0.9 (0.4–4.2)
$\delta^{18}O$ (‰)	−2.9 ± 0.7 (−5.5 to −2.0)	−1.9 ± 0.7 (−3.1 to −1.2)	−3.3 ± 0.3 (−3.6 to −2.4)	−3.7 ± 0.2 (−4.0 to −3.5)	−3.0 ± 0.9 (−12 to −4)	−0.9 ± 0.8 (−3.6 to −1.5)	−0.9 ± 0.9 (−3.5 to −1.0)	−0.9 ± 0.8 (−3.6 to −1.5)	−1.4 ± 0.8 (−4.7 to −0.1)	−1.3 ± 0.7 (−4.8 to −0.3)	−1.4 ± 0.8 (−4.8 to −0.1)
Chl*a* (μg/L)		7.9 ± 6.5 (0.4–18.8)	0.1 ± 0.0 (0.0–0.2)	0.0 ± 0.0 (0.0–0.1)	2.7 ± 5.3 (0.0–18.8)						

Transect 1 were different from Transects 2 and 3, with higher ($p<0.05$) a_{440} values and lower ($p<0.05$) spectral slopes than Transects 2 and 3 (Table 1 and Fig. 4). In comparison to the 2010 values, a_{254} and a_{440} from Transect 1 in 2011 were similar ($p>0.05$), whereas $S_{350-400}$ and $S_{275-295}$ were lower ($p<0.05$) than in 2010.

3.2. Physical and biogeochemical properties

Bare ice cores and those below melt ponds had statistically similar ($p>0.05$) $\delta^{18}O$ values, but salinity was significantly higher ($p<0.05$) in bare ice cores (Table 1 and Fig. 5) potentially owing to brine channel drainage in the melt pond ice cores. In addition, these properties were relatively consistent throughout each ice core with the exception of $\delta^{18}O$, which showed considerable variation within several ice cores (Fig. 5). Comparing the cores from 2010 to those sampled in 2011, the 2011 cores had significantly higher ($p<0.05$) salinity and $\delta^{18}O$ values.

Within the under-ice water samples, both the average salinity and $\delta^{18}O$ values were similar ($p>0.05$) between years and fairly consistent throughout the water column, however there was a larger range in salinity and $\delta^{18}O$ in 2010 owing to strong stratification in the upper few meters of the water column (Table 1 and Fig. 6). Salinity, $\delta^{18}O$ and Chl*a* were higher ($p<0.05$) in the westernmost transect than in the other two transects to the east in 2011, consistent with expected water mass associations (Table 1 and Fig. 6). As would be expected, salinity was lower ($p<0.05$) (while $\delta^{18}O$ was higher ($p<0.05$)) in the ice cores compared to the underlying water column for both 2010 and 2011.

3.3. Comparing optical, physical and biogeochemical properties

The CDOM absorbance coefficients a_{254} and a_{440} exhibited the most significant differences between the more saline water column samples and the CDOM from the fresher sea ice and melt pond samples (Fig. 7). In general, the under-ice waters had higher CDOM absorption than the overlying ice cores. The samples from the interface waters (0 m) in both years showed a range in both salinity and absorbance coefficients (Figs. 4, 6 and 7), likely indicating a progression of ice melt mixing with the upper layers of the water column.

In the 2011 under-ice waters, optical and biogeochemical properties varied among the three transects. In particular, Chl*a*, a_{440} and $S_{350-400}$ showed statistically significant differences ($p<0.05$) between Transect 1, and Transects 2 and 3 (Figs. 4 and 6). Average Chl*a* values for Transects 2 and 3 were 0.1 and <0.1 μg/L, respectively; whereas in Transect 1, Chl*a* was significantly higher ($p<0.05$), with an average value of 7.9 μg/L and a maximum of 18.8 μg/L. This also corresponded with higher a_{440} and lower $S_{350-400}$ values ($p<0.05$). However, for Transect 1 (where Chl*a* also varied over a large range), there does not appear to be a direct relationship with either of these CDOM optical properties (Fig. 8).

The highest a_{440} values in 2011 were measured in the surface waters of the southernmost station (station 55) in Transect 1 (Fig. 9a). In the same location, there is higher salinity (31.4–32.0, Fig. 9d) and the $\delta^{18}O$ value is close to that of sea ice (−1‰) (Fig. 9c). Chl*a* is high at this location as well, but the highest Chl*a* values were observed at station 56 (Fig. 9b). From this cross-sectional view, it is clear that although both Chl*a* and a_{440} were higher in Transect 1, there is not a linear relationship between these two variables.

Please cite this article as: Logvinova, C.L., et al., The potential role of sea ice melt in the distribution of chromophoric dissolved organic matter in the Chukchi and Beaufort Seas. Deep-Sea Res. II (2016), http://dx.doi.org/10.1016/j.dsr2.2016.04.017

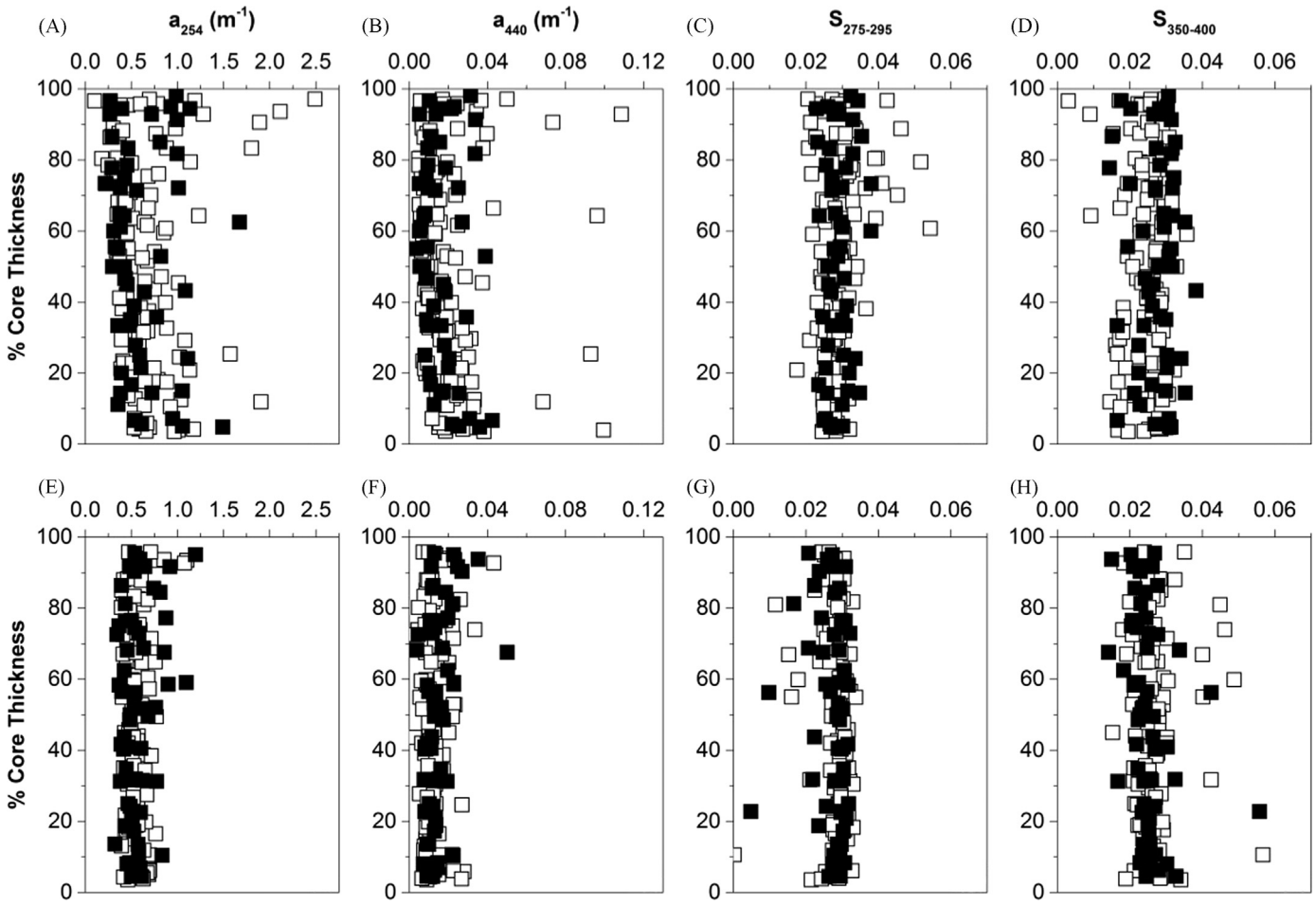

Fig. 3. Ice core profiles of optical properties from bare ice cores (white) and melt pond ice cores (black) from 2010 (a–d) and 2011 (e–h). Ice cores varied in length, so for consistency samples are plotted by percent core thickness relative to the bottom of each core for consistency, with 0% representing the bottom of the ice core and the ice–water interface.

3.4. Sea ice melt

An analysis of the estimated sea ice melt fraction for each of the 2011 water samples was made by solving three simultaneous equations for a simplified Arctic surface water mixing system that includes sea ice melt (SIM), Atlantic water (AW) and meteoric water (MW).

$$\delta^{18}\mathrm{O} = (-1‰ \times f_{\mathrm{SIM}}) + (0.3‰ \times f_{\mathrm{AW}}) + (-21.35‰ \times f_{MW})$$

$$\mathrm{Sal} = (4 \times f_{\mathrm{SIM}}) + (34.8 \times f_{\mathrm{AW}}) + (0 \times f_{\mathrm{MW}})$$

$$f_{\mathrm{SIM}} + f_{\mathrm{AW}} + f_{\mathrm{MW}} = 1$$

where δ^{18}O is the oxygen isotope value of the water sample, Sal is the salinity of the water sample and f is estimated fraction of SIM, AW or MW. Based upon our extensive measurements of sea ice during the ICESCAPE cruises, the average salinity for SIM was 4 and the average δ^{18}O value was −1‰. Based on observations of the core Atlantic water in the Arctic Ocean from Ekwurzel et al. (2001), a salinity of 34.8 and a δ^{18}O value of 0.3‰ were chosen for AW. Because the under-ice waters were largely influenced by water flowing north through the Bering Strait (Weingartner et al., 2005; Spall et al., 2014), for meteoric water we chose a runoff end-member for δ^{18}O of −21.35‰, which corresponds to the most up-to-date data for the freshwater end-member (salinity=0) present in waters collected solely within Bering Strait (Cooper et al., 2006 and unpublished data). Salinity and δ^{18}O values are summarized in Table 2.

Solving the three simultaneous equations shows sea ice melt is present in the 2011 under-ice waters with fractions ranging from −0.05 to 0.5. Note that negative sea ice melt fractions correspond to brine injection from sea ice during formation and early stages of melt, which also suggests that the positive fractions of melted sea ice are likely underestimates of actual melt water fractions (Cooper et al., 2005). The average value for the sea ice melt fraction was lower in Transect 1 than in Transects 2 and 3. Depth profiles of f_{SIM} (Fig. 10), as would be expected, exhibit the highest values near the bottom of the ice. In Transect 1, many f_{SIM} values were negative, indicating a strong presence of sea ice brine. Comparing f_{SIM} to CDOM optical properties, negative f_{SIM} values from the westernmost transect corresponded to higher a_{440} values and lower CDOM spectral slopes (Fig. 11).

3.5. Fluorescence and PARAFAC analysis

EEMs from all three transects in 2011 exhibited a broad emission spectra around and above 400 nm, which is typical of humic DOM (Coble, 2007). The EEMs also exhibited spectra resembling amino acid-like DOM with a local maximum in the emission spectra located below 400 nm (Coble, 2007). However, the EEMs from Transect 1 exhibited additional peaks with excitation maxima between 290 and 310 nm and emission maxima between 370 and 410 nm. This has been previously identified as a marine humic signal (Coble, 2007) (Fig. 12, Table 3).

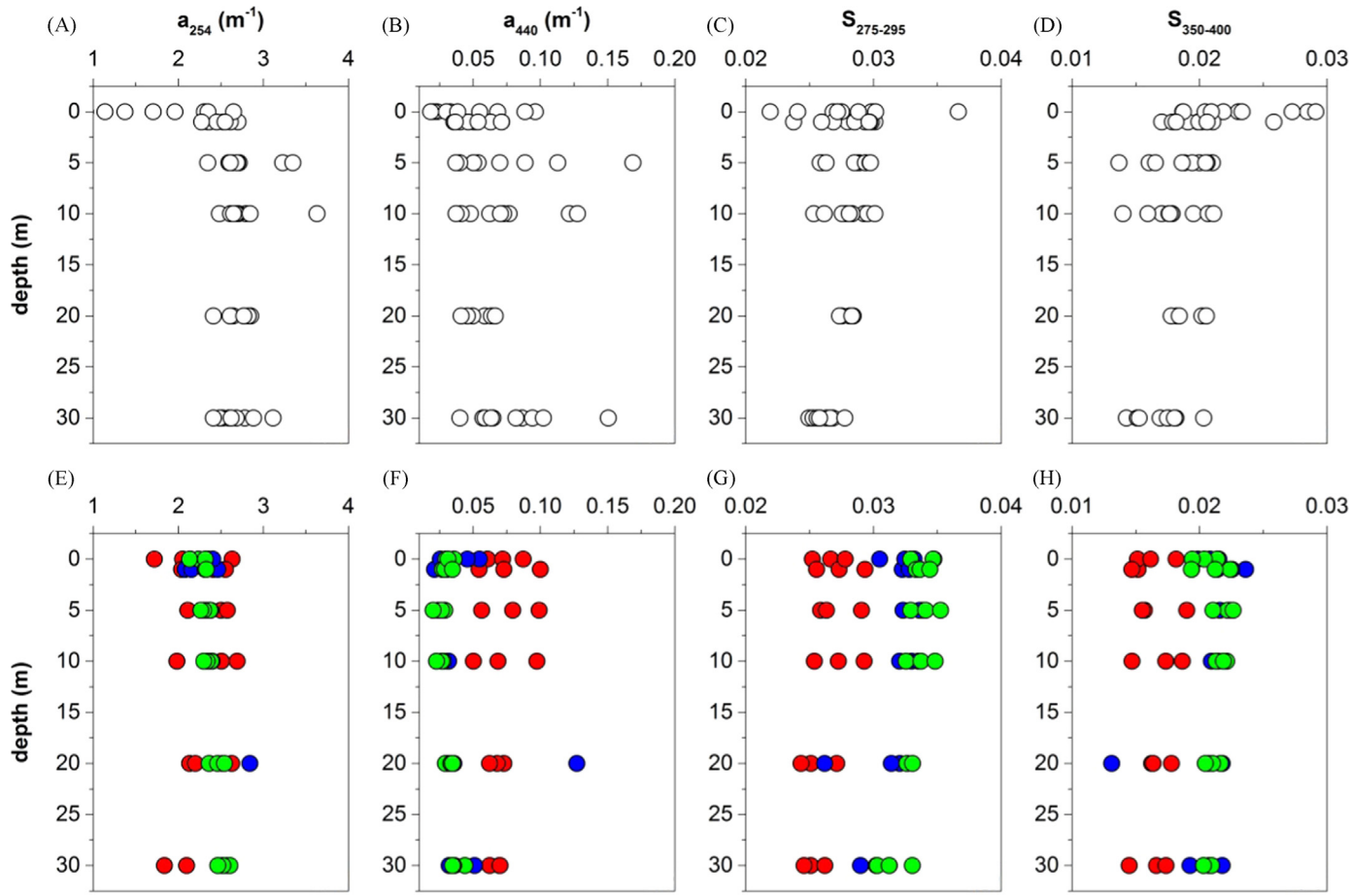

Fig. 4. Optical properties plotted by depth for water samples from 2010 (white, a–d) and the three transects in 2011 (e–h): Transect 1 (red), Transect 2 (blue) and Transect 3 (green). (For interpretation of the references to color in this figure legend, the reader is referred to the web version of this article.)

Three independent fluorescent components were validated for FDOM using PARAFAC analyses (Fig. 13). We compared the spectral characteristics of these components to previously identified components identified in prior studies in order to identify potential sources for each of the three components (Table 4). All components identified were similar to those found in a global study of marine DOM by Jørgensen et al. (2011), indicating that the components identified here are typical of a wide range of marine waters. Components 1 and 3 had spectra resembling humic-like DOM, with broad emission spectra around and above 400 nm and a broader excitation spectra compared to the second component. Component 1 exhibits characteristics of the fulvic acid fluorophore group and could represent terrestrially-derived or autochthonous material (Stedmon and Markager, 2005a; Walker et al., 2009). Component 3 has also been identified as being humic-like and is marine derived or anthropogenic (Stedmon and Markager, 2005a). Component 2 exhibited spectra resembling amino acid-like DOM, with emission spectra maxima below 400 nm. It most closely resembles tyrosine (Stedmon and Markager, 2005a), which is microbially produced in marine waters (Coble, 1996; Stedmon and Markager, 2005b).

There were trends in the distribution of these components. Components 1 and 3 were significantly higher ($p < 0.05$) in Transect 1 compared to Transects 2 and 3, whereas component 2 (the protein-like fluorescence) was similar ($p > 0.05$) for all water samples and had a consistently low contribution (Fig. 14). Both humic-like components (components 1 and 3) showed significant positive relationships with f_{AW} (Fig. 15) but there was no apparent relationship between f_{AW} and protein-like component 2 (not shown).

4. Discussion

4.1. CDOM optical properties

The absorption coefficient at 440 nm measured in the under-ice water at our sites in the Chukchi and Beaufort Seas were in the range expected of Arctic waters (Matsuoka et al., 2011). In a study by Matsuoka et al. (2011), a_{440} varied widely (0.0046–0.5 m^{-1}) in the western Arctic and fell mostly within the range observed for European coastal waters (Babin et al., 2003), with the exception of the lowest values that are consistent with open oceanic waters (*e.g.*, 0.004 m^{-1}) in the western Greenland Sea (Kirk, 1994). In this study, we observed a relatively small range in a_{440} (0.02–0.17 m^{-1}, Table 1) with an average value of 0.06 m^{-1} in 2010 and 0.05 m^{-1} in 2011 which are similar to the mean value of 0.05 m^{-1} observed by Matsuoka et al. (2011).

Several of the water and sea ice samples in our study had CDOM absorption spectra that differed from the typical exponential decay and instead exhibited distinct shoulders and peaks in the 260–400 nm spectral range (Fig. 2). Similar CDOM absorption spectra have been observed in marine, sea ice and sea ice brine samples from other studies and are likely associated with mycosporine-like amino acids (MAAs) and aromatic amino acids (AAAs) (Belzile et al., 2000; Whitehead and Vernet, 2000; Uusikivi et al., 2010; Norman et al., 2011) that function to protect marine organisms against harmful effects of UV radiation. In 2010 shoulders and peaks in the CDOM absorption spectra were observed in both the ice cores and in the under-ice water samples from the interface and 1 m below the ice, but in 2011 these

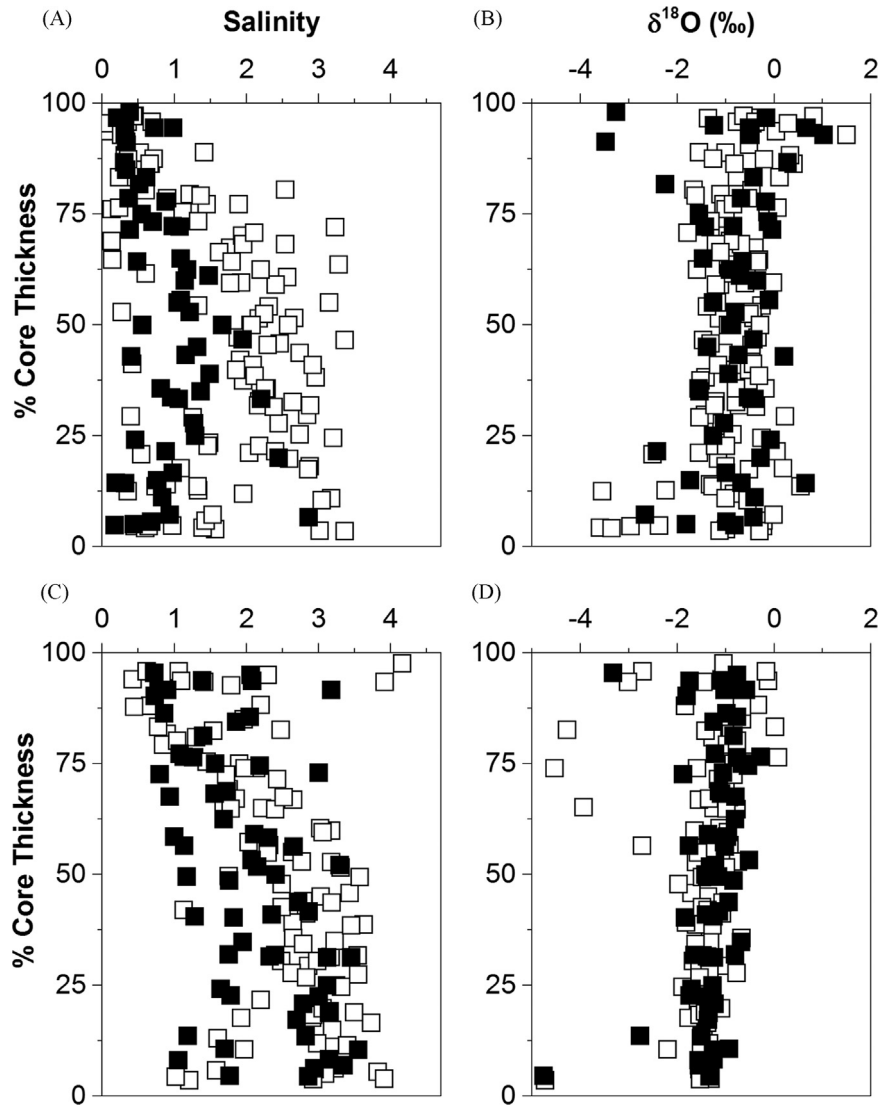

Fig. 5. Salinity and $\delta^{18}O$ for bare ice cores (white) and melt pond ice cores (black) from 2010 (a,b) and 2011 (c,d). Ice cores varied in length so samples are plotted by percent core thickness relative to the bottom of each core for consistency, with 0% representing the bottom of the ice core and the ice–water interface.

anomalies in absorbance were only observed in the ice core samples. Several of the interface water samples from 2010 were fresher and had more negative $\delta^{18}O$ values than interface samples from 2011 (Fig. 6), indicating that there was more sea ice melt in the interface water in 2010. The fact that the shoulders and peaks were only observed in sea ice and under-ice water samples with a higher proportion of sea ice melt, suggests that these MAA and AAA signals are somehow associated with sea ice and only enter the water column when sea ice melts. One possibility is that the MAA and AAAs were produced by sea ice algae (Ryan et al., 2002; Uusikivi et al., 2010; Mundy et al., 2011) that are often found at the bottom of sea ice at the ice–water interface (Melnikov et al., 2002).

4.2. Sea ice as a source of CDOM

In this study, CDOM absorption coefficients in the ice core samples were lower than in the underlying water column, indicating lower concentrations of CDOM in the sea ice. In contrast, several previous studies in the Baltic (Ehn et al., 2004; Granskog et al., 2005; Stedmon et al., 2007a; Uusikivi et al., 2010), the Canadian Arctic (Belzile et al., 2000, Scully and Miller, 2000), and Antarctica (Norman et al., 2011) observed high levels of CDOM in sea ice suggesting that sea ice algae can act as a significant source of CDOM to the underlying water column. For example, Scully and Miller (2000) observed a_{310} values in sea ice cores collected near the North Water polynya that were an order of magnitude greater than those observed in the underlying water, leading them to conclude that sea ice algae is a significant source of CDOM upon sea ice melt in Baffin Bay.

The low CDOM absorption in our sea ice samples could be an artifact of the timing of sampling. Most of the sea ice algal biomass is typically located in the bottom 2 cm of the ice (Belzile et al., 2000; Melnikov et al., 2002; Cooper et al., 2013) and, as a result, most of the CDOM is located at the bottom of the ice core with the rest of the core containing considerably less CDOM than the underlying water column (Belzile et al., 2000; Scully and Miller, 2000). Analysis of the salinity and $\delta^{18}O$ profiles suggests that the ice had reached an advanced state of melt when we made our observations in both 2010 and 2011 (Polashenski et al., 2015; Cooper et al., 2016, this issue); therefore, the high CDOM bottom layer may have already melted. Overall, our observations suggest that sea ice in this region does not act as a source of CDOM during the June–July melt period, but rather dilutes the under-ice water column CDOM during this later stage of melt.

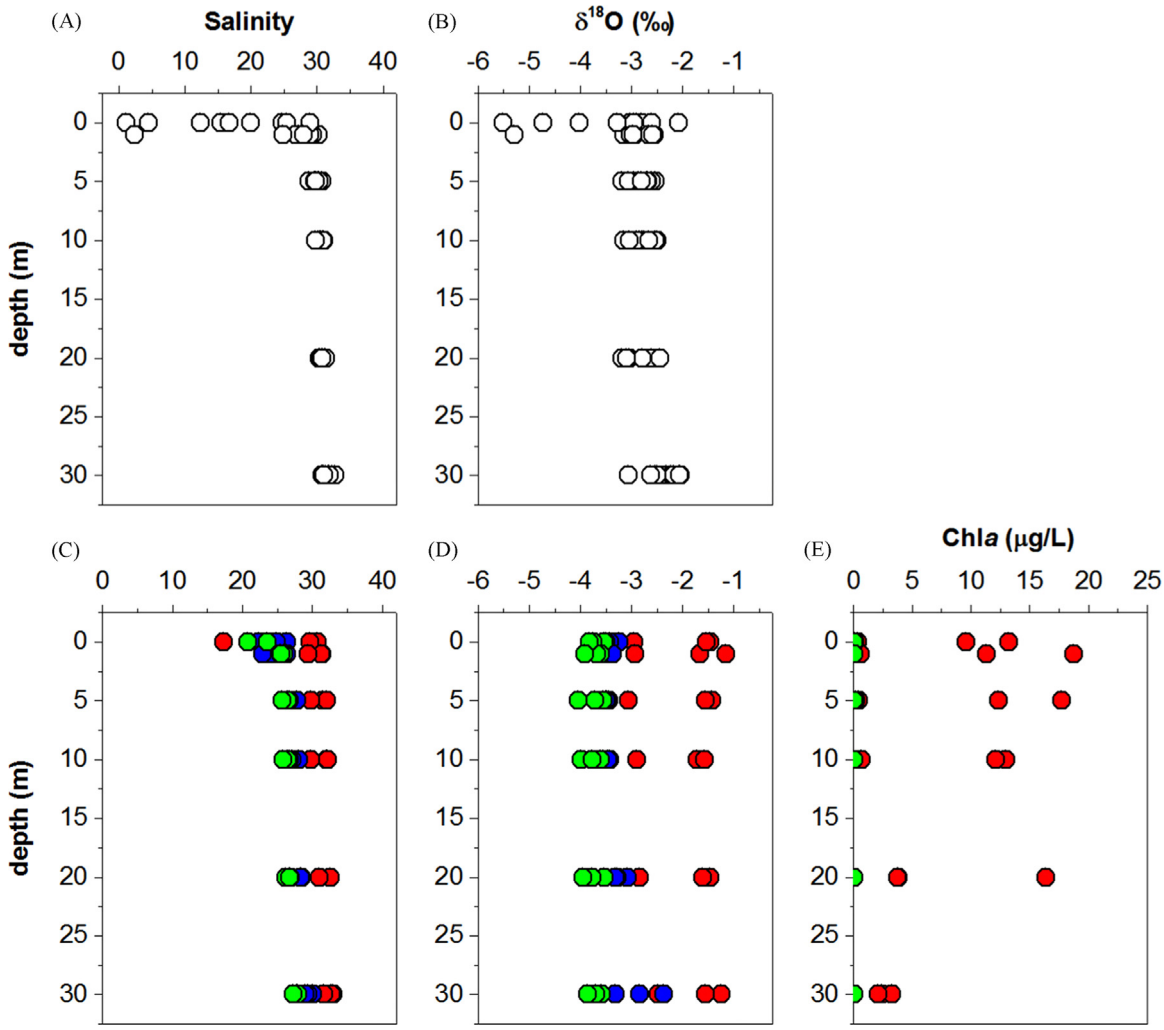

Fig. 6. Salinity and $\delta^{18}O$ for under-ice water samples from 2010 (white, a,b) and salinity, $\delta^{18}O$ and Chl*a* for under-ice water samples from the three transects in 2011(c–e): Transect 1 (red), Transect 2 (blue), and Transect 3 (green). (For interpretation of the references to color in this figure legend, the reader is referred to the web version of this article.)

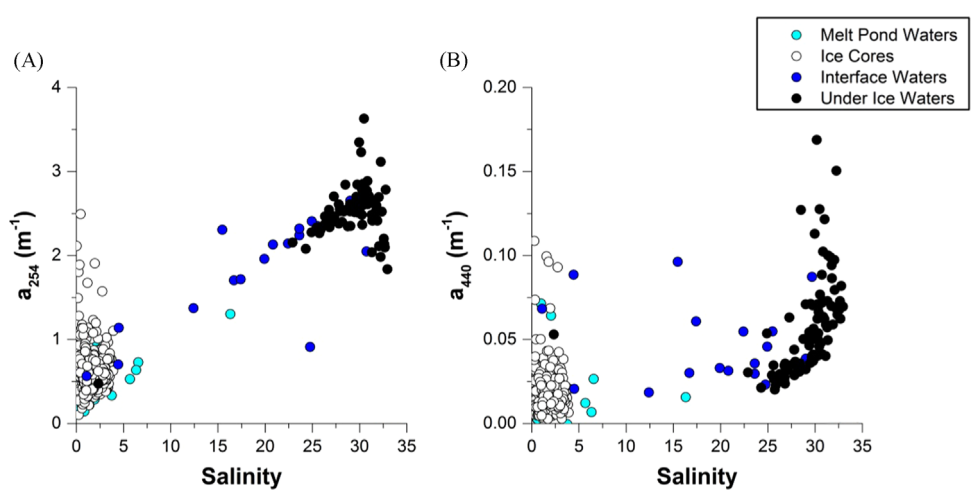

Fig. 7. a_{254} (a) and a_{440} (b) as a function of salinity for melt pond waters, ice cores, interface waters and under-ice waters.

4.3. Potential sources of high CDOM in under-ice waters

The under-ice water column samples collected in 2011 for the three stations in Transect 1 exhibited higher absorbance values than those observed in Transects 2 or 3 (Table 1 and Fig. 4), indicating higher concentrations of CDOM at these first three stations. There are several possible sources of this higher CDOM: river discharge, melted sea ice, and *in situ* autochthonous production.

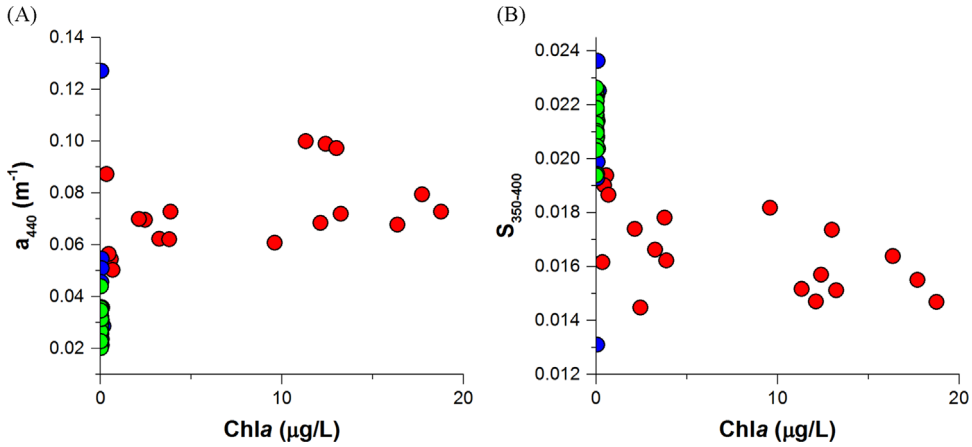

Fig. 8. a_{440} (a) and $S_{350-400}$ (b) as a function of chlorophyll-*a* (Chl*a*) for samples across the three 2011 transects: Transect 1 (red), Transect 2 (blue), and Transect 3 (green). No Chl*a* data were collected in 2010. (For interpretation of the references to color in this figure legend, the reader is referred to the web version of this article.)

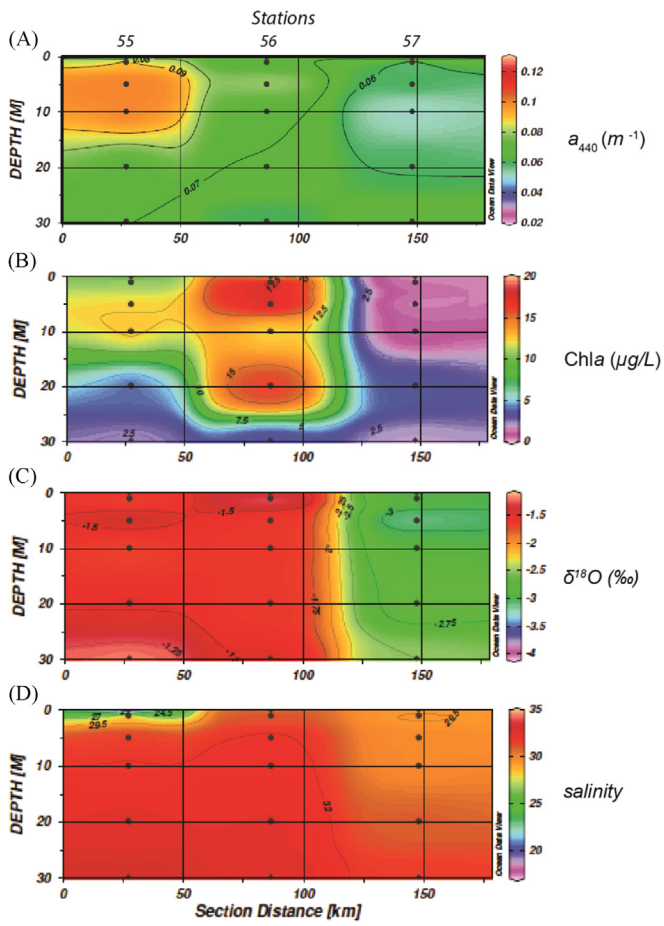

Fig. 9. a_{440} (a), Chl*a* (b), $\delta^{18}O$ (c) and salinity (d) for under-ice waters from the western transect (Transect 1) in 2011. Section orientation is from south to north. Ocean Data View (Schlitzer, 2014).

Table 2
Values of salinity and $\delta^{18}O$ for end-members used in the mass balance equations.

	Sea ice melt (SIM)	Atlantic water (AW)	Meteoric water (MW)
Salinity	4	34.8	0
$\delta^{18}O$	−1	0.3	−21.35

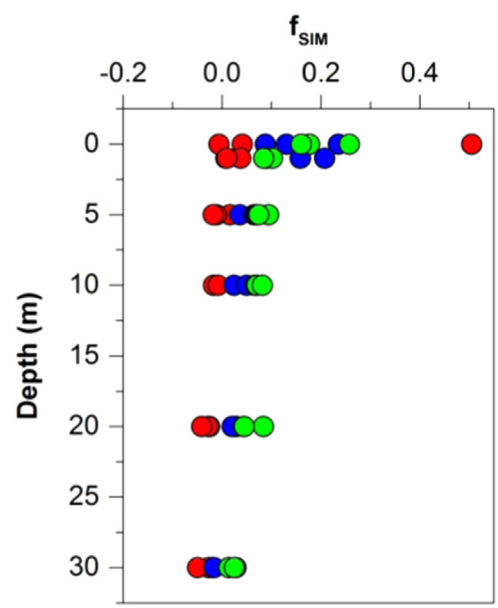

Fig. 10. Sea ice melt fraction for 2011 under-ice waters: Transect 1 (red), Transect 2 (blue) and Transect 3 (green). Negative sea ice melt fraction corresponds to brine injection from sea ice during formation and early stages of melt. (For interpretation of the references to color in this figure legend, the reader is referred to the web version of this article.)

Terrestrial runoff supplies a significant proportion of the CDOM in the Arctic Ocean (Lobbes et al., 2000; Griffin et al., 2011, Stedmon et al., 2011). Negative relationships are commonly observed between CDOM absorption and salinity when runoff is the dominant source of this allochthonous CDOM (Blough and Del Vecchio, 2002). We did not observe this in our water column samples, but rather the highest CDOM absorption was associated with the highest salinities (Fig. 7). Compared to Transects 2 and 3, Transect 1 also exhibited a lower fraction of meteoric water (Fig. 10, Table 3). Therefore, it is not likely that riverine DOM was the dominant source of the anomalously high CDOM signals we observed in Transect 1 during 2011.

During the ICESCAPE mission in 2011, a significant under-ice phytoplankton bloom was observed within Transect 1 (Arrigo et al., 2012, 2014), which could be related to our observed high CDOM absorption. The samples in Transect 1 exhibited lower absorbance spectral slopes suggesting the presence of higher molecular weight material that may have been recently produced. Prior work in the open waters of the Chukchi Sea showed a direct relationship between higher a_{440} and higher Chl*a* concentrations

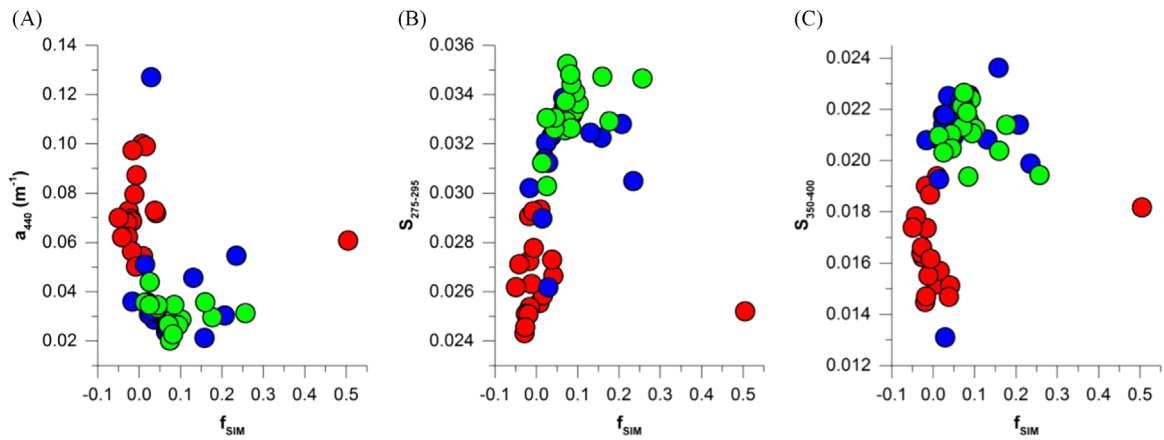

Fig. 11. a_{440} (a), $S_{275–295}$ (b) and $S_{350–400}$ (c) as a function of sea ice melt fraction for the 2011 samples for the three transects: Transect 1 (red), Transect 2 (blue) and Transect 3 (green). Negative sea ice melt fraction corresponds to brine injection from sea ice during formation and early stages of melt. (For interpretation of the references to color in this figure legend, the reader is referred to the web version of this article.)

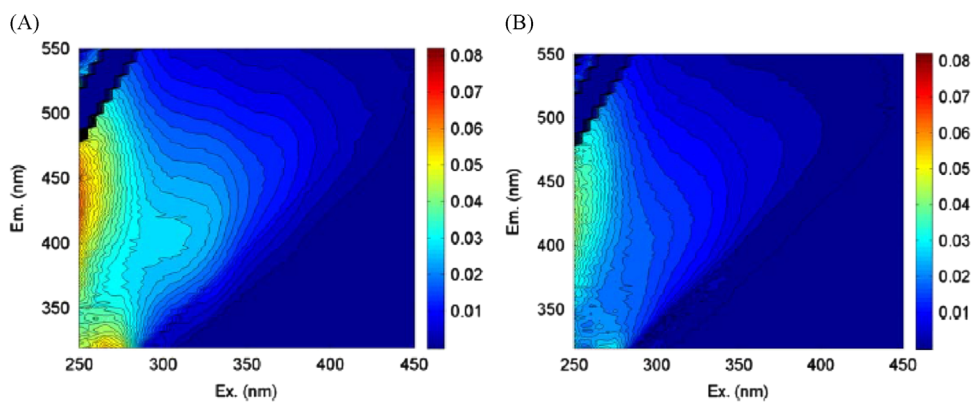

Fig. 12. Representative EEMs from Transect 1 (a) and Transect 3 (b) from the 2011 under-ice samples.

within two phytoplankton blooms (Pegau, 2002). In our study, Transect 1 showed higher levels of both Chl*a* and a_{440} overall compared to Transects 2 or 3 (Figs. 4 and 6); however, within Transect 1 there was an offset between Chl*a* concentrations and a_{440} with the highest Chl*a* concentrations observed at station 56, whereas the highest a_{440} values were observed at station 55 closer to the ice edge (Figs. 8 and 9). A similar offset between Chl*a* and a_{440} was observed in Funka Bay near Japan, where absorption by CDOM increased when the bloom ended, which indicated that the CDOM increase was the result of microbial activity (Sasaki et al., 2005). Microbes are ubiquitous in the ocean and are known producers of CDOM, and the generation of CDOM in our study could be the result of bacterial processing of algal exudates at the end of the observed phytoplankton bloom (Nelson et al., 1998, 2004; Garneau et al., 2008; Ortega-Retuerta et al., 2009; Lovejoy, 2014). Further support for a marine/autochthonous origin of the higher CDOM absorption measured in Transect 1 is provided by the EEM and PARAFAC analysis. Component 3, which represents marine humic-like material, is higher in Transect 1 compared to Transects 2 or 3. Component 1 is higher in Transects 1 as well, and although it could either be marine or terrestrially-derived, the positive relationship with the fraction of Atlantic water (Fig. 15) suggests that it is more influenced by its marine source than by terrestrial runoff.

Sea ice melt is a third potential source of the anomalously high a_{440} values in the underlying water. As previously mentioned, a_{440} at the time of observation was considerably lower in the sea ice than in the under-ice water column. Additionally, $S_{350–400}$ was higher in the ice, suggesting lower molecular weight material.

Table 3
Average fractions of sea ice melt (f_{SIM}), atlantic water (f_{AW}) and meteoric water (f_{MW}) for the three transects in 2011.

	f_{SIM}	f_{AW}	f_{MW}
Transect 1	0.020	0.877	0.103
Transect 2	0.073	0.765	0.162
Transect 3	0.087	0.731	0.182

However, it is possible that higher CDOM absorption and higher molecular weight material were present in the bottom of the ice earlier in the season or in the sea ice brines and had already melted into the underlying water. Throughout the under-ice water column in Transect 1, the $\delta^{18}O$ values were close to the average value for sea ice (−1‰) which suggests a significant contribution from sea ice melt. Additionally, the f_{SIM} values were largely negative; suggesting that much of the sea ice melt contribution was in the form of sea ice brines that drain from the ice during early stages of melt (Polashenski et al., 2015). Norman et al. (2011) found that CDOM in brine samples from Antarctic sea ice were 4 times higher than underlying seawater further suggesting that brine channel drainage in the early stages of sea ice melt prior to our sampling could be contributing to the higher CDOM that we observed in Transect 1 in 2011.

5. Conclusions and implications

Our observations suggest several possible roles for sea ice in the distribution of CDOM in the Chukchi and Beaufort Seas. CDOM

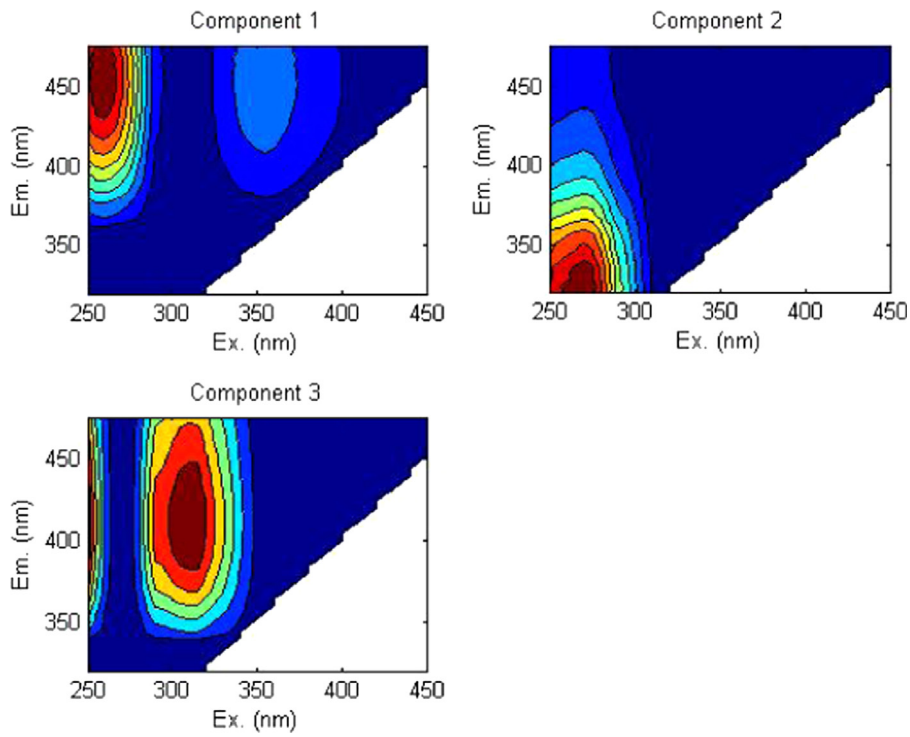

Fig. 13. The three individual components for the PARAFAC model.

Table 4
Spectral characteristics of the six components identified by PARAFAC compared to previously identified components. Secondary maxima are shown in parentheses.

Components	Excitation maxima (nm)	Emission maxima (nm)	Other studies	Description
1	260(355)	452	C1 (Jørgensen et al., 2011) Component 1 (Logvinova et al., unpublished) Component 4 (Stedmon and Markager, 2005a) Component 1 (Stedmon et al., 2007a, 2007b) BERC 1 (Walker et al., 2009) Component 1 (Yamashita et al., 2010)	humic-like, terrestrial/ autochthonous
2	270	324	C5 (Jørgensen et al., 2011) Component 4 (Logvinova et al., unpublished) Component 1 (Murphy et al., 2006) Component 5 (Murphy et al., 2008) Component 8 (Stedmon and Markager, 2005a) Component 4 (Yamashita et al., 2010)	amino acid-like, tyrosine
3	< 250/310	412	C4 (Jørgensen et al., 2011) Component 6 (Logvinova et al., unpublished) Component 6 (Stedmon and Markager, 2005a) Component 2 (Stedmon et al., 2007a) Component 3 (Stedmon et al., 2007b) Component 2 (Yamashita et al., 2010)	humic-like, marine

was higher in the under-ice water samples compared to the overlying sea ice, indicating that sea ice was not directly contributing CDOM to the under-ice water column during the months of June and July. The possibility remains however that CDOM is contributed earlier in the melt season and that it declines by dilution as remnant ice melts (Cooper et al., 2005). The highest CDOM absorption was observed in the under-ice water samples from the first transect in 2011. For this transect, oxygen isotope analysis indicated a significant amount of sea ice melt and brine channel drainage was present in this area, suggesting that sea ice melt that occurred prior to sampling may have contributed CDOM to the underlying water column. This anomalously high CDOM may have also been the result of bacterial activity following the under-ice phytoplankton bloom that was observed in this transect. As sea ice melts and melt pond coverage increases, more light is transmitted through the ice (*e.g.*, Frey et al., 2011), which may stimulate more under-ice phytoplankton blooms that may in turn produce associated autochthonous CDOM. Therefore, if sea ice decline continues in the future, one implication could be an increase in concentrations of CDOM present in the upper ocean water column below sea ice.

Increases in CDOM concentrations could have several effects in the western Arctic Ocean. CDOM plays a significant role in the heat budget of the surface waters of the Chukchi Sea (Hill, 2008), so more CDOM directly below the ice may trap heat that will cause further sea ice melt. As sea ice declines, even more light would be transmitted to the underlying water column. This could potentially further increase primary production and subsequent microbial production of CDOM in ocean surface waters. Additionally, photodegradation can alter the bioavailability of DOM, potentially making it more labile and allowing it to be consumed by bacteria and re-mineralized (*cf.* Mopper et al., 2014). Therefore, this increase in CDOM aligned with enhanced light availability could also ultimately result in an increase in mineralization of organic carbon to atmospheric CO_2 in the Pacific Arctic region.

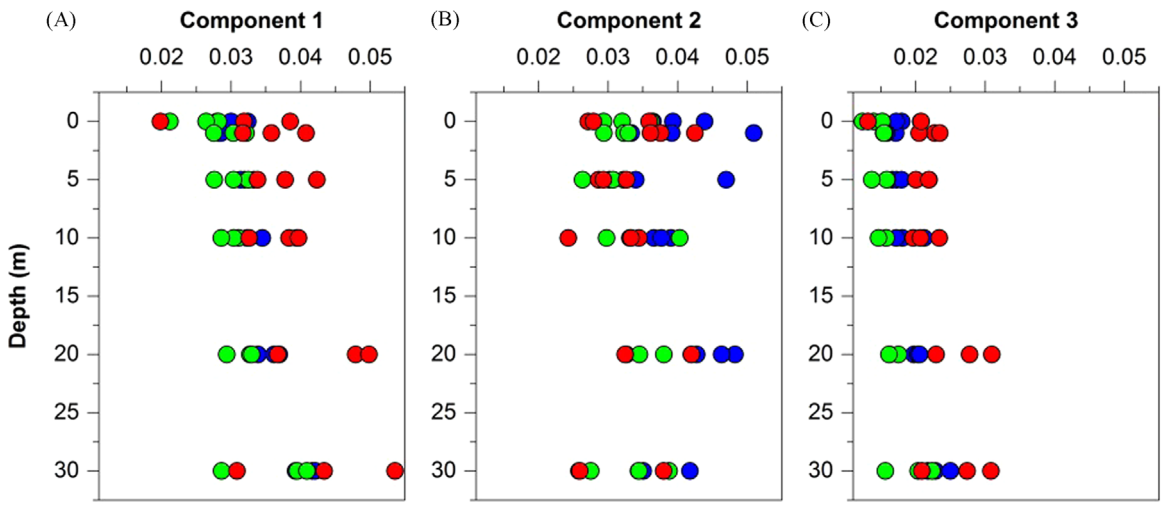

Fig. 14. Loadings for the three PARAFAC components by transect for the 2011 under-ice waters: Transect 1 (red), Transect 2 (blue) and Transect 3 (green). (For interpretation of the references to color in this figure legend, the reader is referred to the web version of this article.)

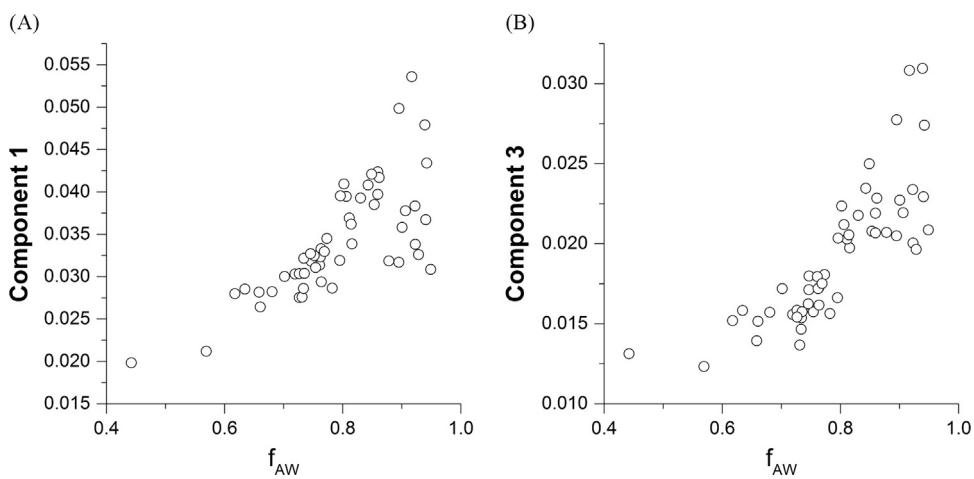

Fig. 15. Components 1 (a) and 3 (b) from the PARAFAC model as a function of Atlantic water fraction.

Acknowledgments

This work was supported through the NASA Impacts of Climate Change on the Ecosystems and Chemistry of the Arctic Pacific Environment (ICESCAPE) project (NASA Cryospheric Sciences Program Grant #NNX10AH71G to K. Frey, L. Cooper, and J. Grebmeier) and the NASA Ocean Biology and Biogeochemistry Program. The field component of this research would not have been possible without the tremendous support from the Commanding Officer, marine science technicians, crew, and officers of USCGC *Healy* on the HLY1001 and HLY1101 missions to the Chukchi and Beaufort seas in June–July of 2010 and 2011. We would also like to thank Holly Kelly, Chris Polashenski and Don Perovich for their help with sample collection.

References

Amon, R., 2004. The role of dissolved organic matter for the organic carbon cycle. In: Stein, R., Macdonald, R.W. (Eds.), The Organic Carbon Cycle in the Arctic Ocean. Springer, New York, pp. 83–99.

Arrigo, K.R., Perovich, D.K., Pickart, R.S., Brown, Z.W., van Dijken, G.L., Lowry, K.E., Mills, M.M., Palmer, M.A., Balch, W.M., Bahr, F., Bates, N.R., Benitez-Nelson, C., Bowler, B., Brownlee, E., Ehn, J.K., Frey, K.E., Garley, R., Laney, S.R., Lubelczyk, L., Mathis, J., Matsuoka, A., Mitchell, B.G., Moore, G.W.K., Ortega-Retuerta, E., Pal, S., Polashenski, C.M., Reynolds, R.A., Schieber, B., Sosik, H.M., Stephens, M., Swift, J.H., 2012. Massive phytoplankton blooms under Arctic Sea ice. Science 336 1408–1408.

Arrigo, K.R., Perovich, D.K., Pickart, R.S., Brown, Z.W., van Dijken, G.L., Lowry, K.E., Mills, M.M., Palmer, M.A., Balch, W.M., Bates, N.R., Benitez-Nelson, C.R., Brownlee, E., Frey, K.E., Laney, S.R., Mathis, J., Matsuoka, A., Mitchell, B.G., Moore, G.W.K., Reynolds, R.A., Sosik, H.M., Swift, J.H., 2014. Phytoplankton blooms beneath the sea ice in the Chukchi Sea. Deep Sea Res. II: Top. Stud. Oceanogr. 105, 1–16.

Babin, M., Stramski, D., Ferrari, G.M., Claustre, H., Bricaud, A., Obolensky, G., Hoepffner, N., 2003. Variations in the light absorption coefficients of phytoplankton, nonalgal particles, and dissolved organic matter in coastal waters around Europe. J. Geophys. Res. 108 (C7), 3211. http://dx.doi.org/10.1029/2001JC000882.

Belanger, S., Xie, H., Krotkov, N., Larouche, P., 2006. Photomineralization of terrigenous dissolved organic matter in Arctic coastal waters from 1979 to 2003: interannual variability and implications of climate change. Glob. Biogeochem. Cycles 20, GB4005. http://dx.doi.org/10.1029/2006GB002708.

Belzile, C., Johannessen, S.C., Gosselin, M., Demers, S., Miller, W.L., 2000. Ultraviolet attenuation by dissolved and particulate constituents of first-year ice during late spring in an Arctic polynya. Limnol. Oceanogr. 45 (6), 1265–1273.

Belzile, C., Gibson, J.A.E., Vincent, W.F., 2002. Colored dissolved organic matter and dissolved organic carbon exclusion from lake ice: implications for irradiance transmission and carbon cycling. Limnol. Oceanogr. 47 (5), 1283–1293.

Blough, N.V., Del Vecchio, R., 2002. Chromophoic DOM in the coastal environment. In: Hansell, D.A., Carlson, C.A. (Eds.), Biogeochemistry of Marine Dissolved Organic Matter. Elsevier, San Diego, California, pp. 509–546.

Bricaud, A., Morel, A., Prieur, L., 1981. Absorption by dissolved organic matter of the sea (yellow substance) in the UV and visible domains. Limnol. Oceanogr. 26 (1), 43–53.

Brown, M., 1977. Transmission spectroscopy examinations of natural waters. Estuar. Coast. Mar. Sci. 5, 309–317. http://dx.doi.org/10.1016/0302–3524(77)90058-5.

Carlson, 2002. Production and removal processes. In: Hansell, D.A., Carlson, C.A. (Eds.), Biogeochemistry of Marine Dissolved Organic Matter. Elsevier, San Diego, California, pp. 91–151.

Coble, P.G., 1996. Characterization of marine and terrestrial DOM in seawater using excitation–emission matrix spectroscopy. Mar. Chem. 51, 325–346.
Coble, P.G., 2007. Marine optical biogeochemistry: the chemistry of ocean color. Chem. Rev. 107, 402–418.
Comiso, J.C., Parkinson, C.L., Gersten, R., Stock, L., 2008. Accelerated decline in the Arctic sea ice cover. Geophys. Res. Lett. 35, L01703. http://dx.doi.org/10.1029/2007GL031972.
Comiso, J.C., 2012. Large decadal decline of the Arctic multiyear ice cover. J. Clim. 25 (4), 1176–1193. http://dx.doi.org/10.1175/JCLI-D-11-00113.1.
Cooper, L.W., Benner, R., McClelland, J.W., Peterson, B.J., Holmes, R.M., Raymond, P. A., Hansell, D.A., Grebmeier, J.M., Codispoti, L.A., 2005. Linkages among runoff, dissolved organic carbon, and the stable isotope composition of seawater and other water mass indicators in the Arctic Ocean. J. Geophys. Res. 110, G02013 1029/2005JG000031.
Cooper, L.W., Codispoti, L.A., Kelly, V., Sheffield, G., Grebmeier, J.M., 2006. The potential for using Little Diomede Island as a platform for observing environmental conditions in Bering Strait. Arctic 59, 129–141.
Cooper, L.W., Sexson, M.G., Grebmeier, J.M., Gradinger, R., Mordy, C.W., 2013. Linkages between sea ice coverage, pelagic–benthic coupling, and the distribution of spectacled eiders: observations in March 2008, 2009, 2010 from the northern Bering Sea. Deep. Sea Res. II: Top. Stud. Oceanogr. 94, 31–43.
Cooper, L.W., Frey, K.E., Logvinova, C.I., Biasatti, D.M., Grebmeier, J.M., 2016. Variations in the contributions of melted sea ice and runoff to surface waters of the Chukchi Sea, 1990-2012 using stable isotope measurements of freshwater endmembers. Deep-sea Research II. http://dx.doi.org/10.1016/j.dsr2.2016.04.017.
Dansgaard, W., 1964. Stable isotopes in precipitation. Tellus 16, 436–468.
Dittmar, T., 2004. Evidence for terrigenous dissolved organic nitrogen in the Arctic deep sea. Limnol. Oceanogr. 49 (1), 148–156.
Ehn, J., Granskog, M.A., Reinart, A., Erm, A., 2004. Optical properties of melting landfast sea ice and underlying seawater in Santala Bay, Gulf of Finland. J. Geophys. Res. 109, C09003. http://dx.doi.org/10.1029/2003JC002042.
Ekwurzel, B., Schlosser, P., Mortlock, R.A., Fairbanks, R.G., Swift, J.H., 2001. River runoff, sea ice meltwater, and Pacific water distribution and mean residence times in the Arctic Ocean. J. Geophys. Res. 106, 9075–9092.
Frey, K.E., Perovich, D.K., Light, B., 2011. The spatial distribution of solar radiation under a melting Arctic sea ice cover. Geophys. Res. Lett. 38, L22501. http://dx.doi.org/10.1029/2011GL049421.
Garneau, M., Roy, S., Lovejoy, C., Gratton, Y., Vincent, W., 2008. Seasonal dynamics of bacterial biomass and production in a coastal arctic ecosystem: Franklin Bay, western Canadian Arctic. J. Geophys. Res. 13. http://dx.doi.org/10.1029/2007JC004281.
Granskog, M.A., Kaartokallio, H., Thomas, D.N., Kuosa, H., 2005. The influence of freshwater inflow on the inorganic nutrient and dissolved organic matter within coastal sea ice and underlying waters in the Gulf of Finland (Baltic Sea). Estuar. Coast. Shelf Sci. 65, 109–122.
Granskog, M.A., Macdonald, R.W., Mundy, C.J., Barber, D.G., 2007. Distribution, characteristics and potential impacts of chromophoric dissolved organic matter (CDOM) in Hudson Strait and Hudson Bay, Canada. Cont. Shelf Res. 27, 2032–2050. http://dx.doi.org/10.1016/j.csr.2007.05.001.
Green, S.A., Blough, N.V., 1994. Optical absorption and fluorescence properties of chromophoric dissolved organic matter in natural waters. Limnol. Oceanogr. 39, 1903–1916.
Griffin, C.G., Frey, K.E., Rogan, J., Holmes, R.M., 2011. Spatial and interannual variability of dissolved organic matter in the Kolyma River, East Siberia, observed using satellite imagery. J. Geophys. Res., 116.
Griffin,C.G., McClelland, J.W., Frey, K.E., Holmes, R.M., 2012. Quantifying and correcting the impacts of freezing samples on dissolved organic matter absorbance. Abstract #B21E-0429, Fall Meeting 2012, American Geophysical Union, San Francisco, 3–7 December.
Helms, J.R., Stubbins, A., Ritchie, J.D., Minor, E.C., Kieber, D.J., Mopper, K., 2008. Absorption spectral slopes, and slope ratios as indicators of molecular weight, source, and photobleaching of chromophoric dissolved organic matter. Limnol. Oceanogr. 53, 955–969.
Hill, V.J., 2008. Impacts of chromophoric dissolved organic material on surface ocean heating in the Chukchi Sea. J. Geophys. Res. 113, C07024. http://dx.doi.org/10.1029/2007JC004119.
Jørgensen, L., Stedmon, C.A., Kragh, T., Markager, S., Middelboe, M., Søndergaard, M., 2011. Global trends in the fluorescence characteristics and distribution of marine dissolved organic matter. Mar. Chem. 126, 139–148. http://dx.doi.org/10.1016/j.marchem.2011.05.002.
Kirk, J.T.O., 1988. Solar heating of water bodies as influenced by their inherent optical properties. J. Geophys. Res. 93 (D9), 10897–10908.
Kirk, J.T.O., 1994. Light and Photosynthesis in Aquatic Ecosystems. Cambridge Univ. Press, Cambridge, U.K.
Kwok, R., Rothrock, D.A., 2009. Decline in Arctic sea ice thickness from submarine and ICESat records: 1958–2008. Geophys. Res. Lett. 36, L15501. http://dx.doi.org/10.1029/2009GL039035.
Lawaetz, A.J., Stedmon, C.A., 2009. Fluorescence intensity calibration using the Raman scatter peak of water. Appl. Spectrosc. 63 (8), 936–940.
Lobbes, J.M., Fitznar, H.P., Kattner, G., 2000. Biogeochemical characteristics of dissolved and particulate organic matter in Russian rivers entering the Arctic Ocean. Geochim. Cosmochim. Acta 64, 2973–2983.
Lovejoy, C., 2014. Changing views of Arctic protists (marine microbial eukaryotes) in a changing Arctic. Acta Protozool. 53, 91–100. http://dx.doi.org/10.4467/16890027AP.14.009.1446.
Markus, T., Stroeve, J.C., Miller, J., 2009. Recent changes in Arctic sea ice melt onset, freezeup, and melt season length. J. Geophys. Res. 114, C12024 10:1029/2009JC005436.
Maslanik, J.A., Fowler, C., Stroeve, J., Drobot, S., Zwally, J., Yi, D., Emery, W., 2007. A younger, thinner Arctic ice cover: increased potential for rapid, extensive sea-ice loss. Geophys. Res. Lett. 34, L24501 10:1029/2007GL032043.
Maslanik, J., Stroeve, J., Fowler, C., Emery, W., 2011. Distribution and trends in Arctic sea ice age through spring 2011. Geophys. Res. Lett. 38, L13502. http://dx.doi.org/10.1029/2011GL047735.
Matsuoka, A., Hill, V., Huot, Y., Babin, M., Bricaud, A., 2011. Seasonal variability in the light absorption properties of western Arctic waters: parameterization of the individual components of absorption for ocean color applications. J. Geophys. Res. 116, C02007. http://dx.doi.org/10.1029/2009JC005594.
Matsuoka, A., Bricaud, A., Benner, R., Para, J., Sempere, R., Prieur, L., Belanger, S., Babin, M., 2012. Tracing the transport of colored dissolved organic matter in water masses of the Southern Beaufort Sea: relationship with hydrographic characteristics. Biogeosciences 9, 925–940 10.5194/bg-9-925-2012.
Melnikov, I.A., Kolosova, E.G., Welch, H.E., Zhitina, L.S., 2002. Sea ice biological communities and nutrient dynamics in the Canada Basin of the Arctic Ocean. Deep Sea Res. I: Oceanogr. Res. Pap. 49, 1623–1649.
Mitchell, B.G., Kahru, M., Wieland, J., Stramska, M., 2003. Determination of spectral absorption coefficients of particles, dissolved material and phytoplankton for discrete water samples. In: Mueller, J.L., Fargion, G.S., McClain, C.R. (Eds.), Ocean Optics Protocols for Satellite Ocean Color Sensor Valida- tion. Revision 4, Vol. IV. NASA/TM-2003-211621/R, Goddard Space Flight Center, Greenbelt, Md., pp. 39–56.
Mopper, K., Kieber, D., Stubbins, A., 2014. The role of photochemistry in the cycling of carbon, sulfur, nitrogen and phosphorous. In: Hansell, Dennis A., Carlson, Craig A. (Eds.), Biogeochemistry of Marine Dissolved Organic Matter, Second Edition Academic Press, New York, pp. 389–450.
Moran, M.A., Zepp, R.G., 1997. Role of photoreactions in the formation of biologically labile compounds from dissolved organic matter. Limnol. Oceanogr. 42, 1307–1316.
Mundy, C.J., Gosselin, M., Ehn, J.K., Belzile, C., Poulin, M., Alou, E., Roy, S., Hop, H., Lessard, S., Papakyriakou, T.N., Barber, D.G., Stewart, J., 2011. Characteristics of two distinct high-light acclimated algal communities during advanced stages of sea ice melt. Polar Biol. 34, 1869–1886. http://dx.doi.org/10.1007/s00300-011-0998-x.
Murphy, K.R., Stedmon, C.A., Waite, T.D., Ruiz, G.M., 2008. Distinguishing between terrestrial and autochthonous organic matter sources in the marine environments using fluorescence spectroscopy. Mar. Chem. 108, 40–58.
Murphy, K.R., Ruiz, G.M., Dunsmuir, W.T.M., Waite, T.D., 2006. Optimized parameters for fluorescence-based verification of ballast water exchange by ships. Environ. Sci. Technol. 40, 2357–2362. http://dx.doi.org/10.1021/es0519381.
Nelson, N.B., Siegel, D.A., Michaels, A.F., 1998. Seasonal dynamics of colored dissolved organic material in the Sargasso Sea. Deep Sea Res. I: Oceanogr. Res. Pap. 45, 931–957.
Nelson, N.B., Siegel, D.A., 2002. Chromophoric DOM in the open ocean. In: Hansell, D.A., Carlson, C.A. (Eds.), Biogeochemistry of Marine Dissolved Organic Matter. Elsevier, San Diego, CA, pp. 547–578.
Nelson, B.N., Carlson, C.A., Steinburg, D.K., 2004. Production of chromophoric dissolved organic matter by Sargasso Sea microbes. Mar. Chem. 89, 273–287. http://dx.doi.org/10.1016/j.marchem.2004.02.017.
Norman, L., Thomas, D.N., Stedmon, C.A., Granskog, M.A., Papadimitriou, S., Krapp, R., Meiners, K.M., Lannuzel, D., van der Merwe, P., Dieckmann, G.S., 2011. The characteristics of chromophoric dissolved organic matter (CDOM) in Antarctic sea ice. Deep Sea Res. Part II Top. Stud. Ocean. 58, 1075–1091. http://dx.doi.org/10.1016/j.dsr2.2010.10.030.
Ortega-Retuerta, E., Frazer, T.K., Duarte, C.M., Ruiz-Halpern, S., Tovar-Sanchez, A., Arrieta, J.M., Reche, I., 2009. Biogeneration of chromophoric dissolved organic matter by bacteria and krill in the Southern Ocean. Limnol. Oceanogr. 54 (6), 1941–1950.
Ortega-Retuerta, E., Reche, I., Pulido-Villena, E., Agusti, S., Duarte, C.M., 2010. Distribution and photoreactivity of chromophoric dissolved organic matter in the Antarctic Peninsula (Southern Ocean). Mar. Chem. 118, 129–139.
Osburn, C.L., Retamal, L., Vincent, W.F., 2009. Photoreactivity of chromophoric dissolved organic matter transported by the Mackenzie River to the Beaufort Sea. Mar. Chem. 115, 10–20. http://dx.doi.org/10.1016/j.marchem.2009.05.003.
Paul, D., Skrzypek, G., Fórizs, I., 2007. Normalization of measured stable isotopic compositions to isotope reference scales–a review. Rapid Commun. Mass Spectrom. 21, 3006–3014.
Pegau, W.S., 2002. Inherent optical properties of the central Arctic surface waters. J. Geophys. Res. 107 (C10), 8035. http://dx.doi.org/10.1029/2000JC000382.
Perovich, D., Meier, W., Tschudi, M., Gerland, S., Richter-Menge, J., 2012. Sea Ice [In Arctic Report Card 2012], 〈http://www.arctic.noaa.gov/reportcard〉.
Polashenski, C., Perovich, D.K., Frey, K.,E., Cooper, L.W., Logvinova, C.I., Dadic, R., Light, B., Kelly, H.P., Trusel, L.D., Webster, M., 2015. Physical and Morphological Properties of Sea Ice in the Chukchi and Beaufort Seas during the 2010 and 2011 NASA ICESCAPE Missions. Deep-sea Research II. http://dx.doi.org/10.1016/j.dsr2.2015.04.006.
Retamal, L., Bonilla, S., Vincent, W.F., 2008. Optical gradients and phytoplankton production in the Mackenzie River and the coastal Beaufort Sea. Polar Biol. 31 (3), 363–379.
Ryan, K.G., McMinn, A., Mitchell, K.A., Trenerry, L., 2002. Mycosporine-like amino acids in Antarctic sea ice algae and their response to UVB radiation. Z. Naturforsch C 57c, 471–477.

Sasaki, H., Miyamura, T., Saitoh, S., Ishizaka, J., 2005. Seasonal variation of absorption by particles and colored dissolved organic matter (CDOM) in Funka Bay, southwestern Hokkaido, Japan. Estuar. Coast. Shelf Sci. 64, 447–458. http://dx.doi.org/10.1016/j.ecss.2005.03.008.

Scully, N., Miller, M.W.L., 2000. Spatial and temporal dynamics of colored dissolved organic matter in the north water polynya. Geophys. Res. Lett. 27, 1009–1011.

Serreze, M.C., Holland, M.M., Stroeve, J., 2007. Perspectives on the Arctic's shrinking sea ice cover. Science 315, 133–1536 10:1126/science.1139426.

Spall, M.A., Pickart, R.S., Brugler, E.T., Moore, G.W.K., Thomas, L., Arrigo, K.R., 2014. Role of shelfbreak upwelling in the formation of a massive under-ice bloom in the Chukchi Sea. Deep. Sea Res. Part II: Top. Stud. Ocean. 105 (0), 17–29.

Spencer, R.G.M., Coble, P.G., 2014. Sample design for organic matter fluorescence analysis. In: P.G., Coble, A., Baker, J.R., Lead, D., Reynolds, R.G.M, Spencer (Eds.), Aquatic Organic Matter Fluorescence. Cambridge University Press, New York, NY, Environmental Chemistry Book Series.

Stedmon, C.A., Markager, S., Bro, R., 2003. Tracing dissolved organic matter in aquatic environments using a new approach to fluorescence spectroscopy. Mar. Chem. 82, 239–254. http://dx.doi.org/10.1016/S0304-4203(03)00072-0.

Stedmon, C.A., Markager, S., 2005a. Resolving the variability of dissolved organic matter fluorescence in a temperate estuary and its catchment using PARAFAC analysis. Limnol. Oceanogr. 50, 686–697.

Stedmon, C.A., Markager, S., 2005b. Tracing the production and degradation of autochthonous fractions of dissolved organic matter using fluorescence analysis. Limnol. Oceanogr. 50 (5), 1415–1426.

Stedmon, C.A., Thomas, D.N., Granskog, M., Kaartokallio, H., Papadimitriou, S., Kuosa, H., 2007a. Characteristics of dissolved organic matter in Baltic coastal sea ice: allochthonous or autochthonous origins? Environ. Sci. Technol. 41, 7273–7279.

Stedmon, C.A., Markager, S., Tranvik, L., Kronberg, L., Slatis, T., Martinsen, W., 2007b. Photochemical production of ammonium and transformation of dissolved organic matter in the Baltic Sea. Mar. Chem. 104, 227–240.

Stedmon, C.A., Bro, R., 2008. Characterizing dissolved organic matter fluorescence with parallel factor analysis: a tutorial. Limnol. Oceanogr. Methods 6, 572–579.

Stedmon, C.A., Amon, R.M.W., Rinehart, A.J., Walker, S.A., 2011. The supply and characteristics of colored dissolved organic matter (CDOM) in the Arctic Ocean: pan arctic trends and differences. Mar. Chem. 124, 108–118. http://dx.doi.org/10.1016/j.marchem.2010.12.007.

Stroeve, J., Holland, M.M., Meier, W., Scambos, T., Serreze, M., 2007. Arctic sea ice decline: faster than forecast. Geophys. Res. Lett. 34, L09501. http://dx.doi.org/10.1029/2007GL029703.

Stubbins, A., Hubbard, V., Uher, G., Law, C.S., Upstill-Goddard, R.C., Aiken, G.R., Mopper, K., 2008. Relating carbon monoxide photoproduction to dissolved organic matter functionality. Environ. Sci. Technol. 42, 3271–3276.

Uusikivi, J., Vähätalo, A.V., Granskog, M.A., Sommaruga, R., 2010. Contribution of mycosporine-like amino acids and colored dissolved and particulate matter to sea ice optical properties and ultraviolet attenuation. Limnol. Oceanogr. 55 (2), 703–713.

Walker, S.A., Amon, R.M.W., Stedmon, C., Duan, S., Louchouarn, P., 2009. The use of PARAFAC modeling to trace terrestrial dissolved organic matter and fingerprint water masses in coastal Canadian Arctic surface waters. J. Geophys. Res. 114. http://dx.doi.org/10.1029/2009JG000990.

Weingartner, T., Aagaard, K., Woodgate, R., Danielson, S., Sasaki, Y., Cavalieri, D., 2005. Circulation on the north central Chukchi Sea shelf. Deep Sea Res. Part II Top. Stud. Ocean. 52, 3150–3174.

Welschmeyer, N.A., 1994. Fluorometric analysis of chlorophyll a in the presence of chlorophyll b and pheopigments. Limnol. Oceanogr. 39, 1985–1992.

Whitehead, K., Vernet, M., 2000. Influence of mycosporine-like amino acids (MAAs) on UV absorption by particulate and dissolved organic matter in La Jolla Bay. Limnol. Oceanogr. 45 (8), 1788–1796.

Williamson, C.E., Neale, P.J., Grad, G., De Lange, H.J., Hargreaves, B.R., 2001. Beneficial and detrimental effects of UV on aquatic organisms: implications of spectral variation. Ecol. Appl. 11 (6), 1843–1857.

Xie, H., Gosselin, M., 2005. Photoproduction of carbon monoxide in first-year sea ice in Franklin Bay, southeastern Beaufort Sea. Geophys. Res. Lett. 32, L12606. http://dx.doi.org/10.1029/2005GL022803.

Yamashita, Y., Cory, R.M., Nishioka, J., Kuma, K., Tanoue, E., Jaffe, R., 2010. Fluorescence characteristics of dissolved organic matter in the deep waters of the Okhotsk Sea and the northwestern North Pacific Ocean. Deep Sea Res. Part II 57, 1478–1485.